Nature of Electronic States in Atomically Thin MoS_2 Field-Effect Transistors

Subhamoy Ghatak,* Atindra Nath Pal, and Arindam Ghosh

Department of Physics, Indian Institute of Science, Bangalore 560 012, India

ABSTRACT We present low-temperature electrical transport experiments in five field-effect transistor devices consisting of monolayer, bilayer, and trilayer MoS_2 films, mechanically exfoliated onto Si/SiO_2 substrate. Our experiments reveal that the electronic states in all films are localized well up to room temperature over the experimentally accessible range of gate voltage. This manifests in two-dimensional (2D) variable range hopping (VRH) at high temperatures, while below ~30 K, the conductivity displays oscillatory structures in gate voltage arising from resonant tunneling at the localized sites. From the correlation energy (T_0) of VRH and gate voltage dependence of conductivity, we suggest that Coulomb potential from trapped charges in the substrate is the dominant source of disorder in MoS_2 field-effect devices, which leads to carrier localization, as well.

KEYWORDS: dichalcogenides · field-effect transistor · MoS_2 · localization · Mott variable range hopping · resonant tunneling · charge impurity scattering

Recently, MoS_2-based dichalcogenides have been of renewed interest due to the possibility of creating atomically thin semiconductor membranes for a variety of applications.[1−4] Being a layered compound, with a weak van der Waal interaction between the layers, MoS_2 can be exfoliated like graphene on insulating substrates. This has recently led to the fabrication of a single-layer MoS_2 field-effect transistor that has a very high on−off ratio due to a finite band gap.[4] It has been demonstrated that the band gap is indirect (≈1.2 eV) for multilayer MoS_2 films but direct (≈1.8 eV) for a single atomic layer,[3] which may lead not only to low-power dissipation electronic devices but also new possibilities in energy harvesting designs. The existence of a band gap can also have serious implications on the charge transport and nature of disorder in MoS_2 films, affecting its ability to screen external potential fluctuations.[5,6] In fact, the mobility ($\lesssim$200 $cm^2/V \cdot s$) of charge carriers in single-layer MoS_2 devices is much lower than that of graphene, which has been attributed to the absence of a band gap in pristine 2D layers of graphene. Our objective here is to explore the nature of disorder and hence that of the electronic states, from the low-temperature electrical transport in MoS_2 films, when the film thickness is downsized from a few to a single molecular layer.

Often, disorder in low-dimensional electron systems arises from extraneous sources, such as local charge distribution that induces a random Coulomb potential on the electrons. This, for example, can be the remote dopant ions in modulation-doped III−V semiconductors[7] or charges trapped in the substrate in the case of graphene.[8] At low carrier densities, the screening of the random Coulomb potential becomes weak, causing carriers to localize and/or charge distribution to become inhomogeneous.[9,10] This would have a direct impact not only on the transport but also on the response of the system to various stimuli including light, stress, *etc.* Although a similar charge-trap-mediated transport has been suggested in thick nanoscale patches of MoS_2,[11] the microscopic picture is far from clear. It is also not known if such a picture would be valid in monolayer or very few layer MoS_2 devices. In this context, our experiments with MoS_2 devices of different thicknesses (see Table 1) reveal that electrons are strongly localized in all cases, which manifest in variable range hopping transport and an inhomogeneity in charge distribution that results in local transport resonances at low temperatures. We suggest that localization is probably due to strong potential fluctuations induced by the randomly occupied charge traps that are located primarily at the MoS_2−substrate interface.

RESULTS AND DISCUSSION

Devices were prepared by standard mechanical exfoliation of bulk MoS_2 on 300 nm SiO_2 on n^{++}-doped silicon substrate using the scotch tape technique.[12,13] The flakes were identified using an optical microscope and characterized *via* Raman spectroscopy and atomic force microscopy (AFM). We present detailed experiments on five devices (see Table 1) of different film thicknesses. In Figure 1c, we show Raman spectra for bulk, trilayer, and single-layer MoS_2 films. We focus on the E^1_{2g} and A_{1g} modes which have been

* Address correspondence to ghatak@physics.iisc.ernet.in.

Received for review July 27, 2011 and accepted September 8, 2011.

Published online September 08, 2011
10.1021/nn202852j

© 2011 American Chemical Society

shown to be sensitive to the number of atomic layers.[3] The position of both modes agrees well with a recent investigation of Raman spectroscopy in thin exfoliated MoS_2 films. The separation of E^1_{2g} and A_{1g} peaks was found to be 23, 21, and 16 −18 cm^{-1} for trilayer, bilayer, and single layer, respectively. For further confirmation of Raman data, we determined the thickness of flakes using contact mode AFM. A line scan across the edge of a single-layer flake (Figure 1d) shows a step of ≈0.7 nm, which compares very well with the thickness of the single MoS_2 layer (≈0.65 nm).

The electrical contacts, designed with electron beam lithography, consisted of thermally evaporated Ti/Au or Au films. The optical image of the MoS3L device is shown in Figure 1a. All measurements were carried out in cryostats under high vacuum (10^{-6} mbar) condition. In all devices, the gate voltage (V_{BG}) was applied only at the doped silicon backgate (see Figure 1b). Measurements were primarily two-probe current measurement using lock-in technique due to very high resistance of these systems, although four-probe devices were fabricated, as well. We found, at high doping concentration, that the contact resistance was negligible near room temperature but increases to about half of the sample resistance below 100 K. Detailed $I_{DS}-V_{DS}$ measurements, where I_{DS} and V_{DS} are the drain−source current and bias, respectively, were conducted to characterize the electrical contacts (see Supporting Information). At low voltages ($|V_{DS}| \lesssim 300$ mV), $I_{DS}-V_{DS}$ values at all V_{BG} and near room temperature were linear for both Ti/Au and Au deposited samples, although we have better linear contact with only Au. These results bear close resemblance to the characteristics reported recently for high-mobility MoS_2 devices.[4] As shown in the Supporting Information, $I_{DS}-V_{DS}$ characteristics become nonlinear at large V_{DS}, particularly at low temperatures (T), although we attribute this to the insulating nature of the devices which causes the nonlinearity. The symmetric nature of $I_{DS}-V_{DS}$ around $V_{DS} = 0$ enables us to eliminate any possibility of Schottky contact in our operating V_{DS} range. This is supported by the observed magnitude of the differential carrier mobility μ ($=(1/C) \times d\sigma/dV_{BG}$), where C is the gate capacitance per unit area (here 1.2×10^{-4} F/m^2 for 300 nm SiO_2), and σ ($=(L/W) \times I/V_{DS}$) is the linear conductivity at low V_{DS}. L and W are the length and width of the MoS_2 channel. In both two- and four-probe geometry, we obtained similar values of mobility, which are typical values reported for MoS_2 transistors[4] on the SiO_2 substrate (see Table 1).

TABLE 1. Details of the Devices:

device	number of layers	contact material	V_{ON}[a]	device area ($L \times W$)[b]	mobility[c]
MoS1La	1	Ti/Au	32	4 × 3	1
MoS1Lb	1	Au	15	2 × 2.5	5
MoS1Lc	1	Au	−5	5 × 8	12
MoS2L	2	Au	−2	2.8 × 2.5	20
MoS3L	3	Ti/Au	−25	4 × 16	10

[a] In volts. [b] Both dimensions in μm. [c] In cm^2/V·s near room temperature.

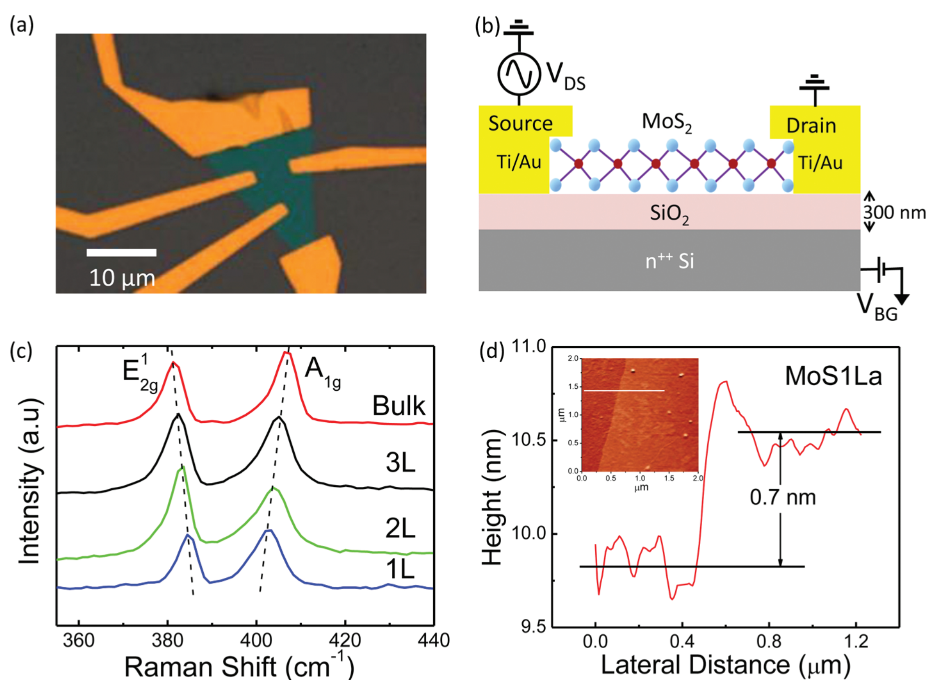

Figure 1. (a) Optical micrograph of a typical MoS_2 device. (b) Schematic of a single-layer MoS_2 field-effect transistor. (c) Raman spectrum of the bulk, trilayer, bilayer, and single-layer MoS_2 films on Si/SiO_2 substrate. (d) Thickness scan along the white line across the boundary of the single-layer MoS_2 in the inset. Inset: High-resolution atomic force microscopy (AFM) image of single-layer MoS_2 film on SiO_2 substrate.

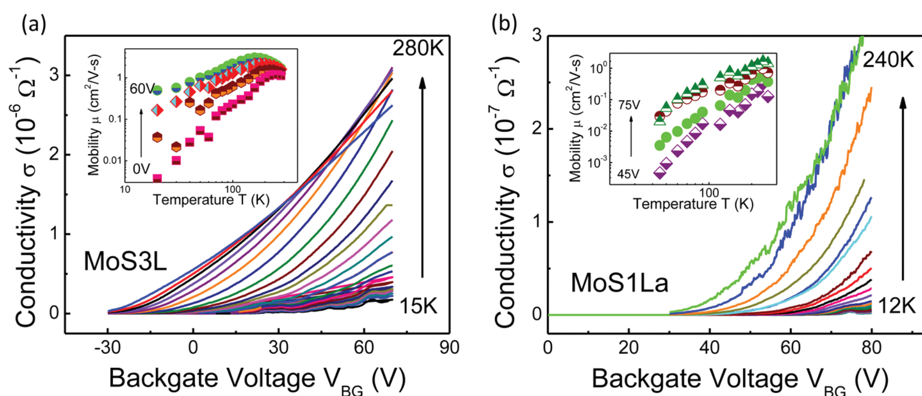

Figure 2. Conductivity σ as a function of backgate voltage (V_{BG}) at various temperatures for (a) MoS3L with V_{DS} = 4 mV and (b) MoS1La with V_{DS} = 100 mV. Insets show corresponding field-effect mobility μ *vs* temperature T at different gate voltages, V_{BG}, extracted from the linear fit of a small region around a particular V_{BG} in σ *vs* V_{BG} graph.

In Figure 2, we show the variation of σ in MoS3L and MoS1La as a function of V_{BG} over a range ~10 to 280 K. The conduction was achieved predominantly in the positive V_{BG} regime, implying that the MoS_2 films were intrinsically n-type.[11] The doping was higher in MoS3L, which required a negative V_{BG} to pinch off completely. Below 250 K, both devices were strongly insulating at all V_g. A weak metal-like behavior was observed at $T > 250$ K and very high doping (large positive V_{BG}) for most of the samples. Such a behavior, which was stronger in MoS3L, was found to be connected to a decrease in μ with increasing T in this regime (inset of Figure 2a,b). This can be attributed to enhanced scattering of electrons by phonons at high temperatures.[14] At low T, both σ and μ drop rapidly with decreasing T. Such an insulating behavior was observed in multilayer nanopatches of MoS_2 (thickness = 8–35 nm), as well,[11] with an apparent activated behavior of σ over a rather limited range of T. This was explained by invoking a dense distribution of trap states, which acted as an "impurity band", although the origin or the physical location of such traps is unclear.

In contrast to the nanopatches,[11] the T dependences of σ in our monolayer and trilayer MoS_2 devices are not activated, but there are two distinct regimes in the T variation in σ (Figure 3a,b): the high T regime ($T \gtrsim 30$ K), where σ increases rapidly with increasing T, and second, the low T regime ($T \lesssim 30$ K), where the variation in σ weakens considerably at most V_{BG} in both devices (except for MoS1La at low V_{BG}, where the weakening of σ sets in at higher T (Figure 3b). We find that, in the high T regime, the variation of σ with T can be modeled very well in terms of variable range hopping (VRH) transport rather than the thermally activated behavior with

$$\sigma = \sigma_0(T)\exp[-(T_0/T)^{1/(d+1)}] \quad (1)$$

where T_0 and d are correlation energy scale and dimensionality,[15,16] respectively, and $\sigma_0 = AT^m$ with $m \approx 0.8$–1. The agreement of the data to VRH transport with $d = 2$ indicates the electron transport in atomically thin MoS_2 occurs in a wide ($\gg k_BT$) band of localized states, rather than direct excitation to conduction band minimum or mobility edge from the Fermi energy as suggested for the nanopatches.[17] The VRH transport in σ also results in ln $\mu \propto T^{-1/3}$ in two dimension.[14] This is confirmed in the inset of Figure 3b for the MoS1La device. The magnitude of T_0 decreases rapidly as V_{BG}, or equivalently, the Fermi energy E_F, is increased. Such a behavior is common to strongly localized 2D electron systems[18,19] and implies that E_F is located in the conduction band tail.

To understand the weakening of σ at $T \lesssim 30$ K, we have magnified this regime for both MoS3L (Figure 3c) and MoS1La (Figure 3d). In both cases, the variation of σ with V_{BG} becomes nonmonotonic and displays several peaks which become progressively well-defined as T is reduced. The peaks are highly reproducible and stable even at $T \sim$ 30–40 K, indicating that random fluctuations due to interference of hopping paths are unlikely to cause them. Resonant tunneling at the localized states in disordered mesoscopic semiconductors is known to result in strong reproducible peaks in σ at low temperatures.[20,21] In the presence of multiple overlapping resonances, T dependence of σ weakens, as observed in our data.[21] However, confirmation of this scenario can be obtained by shifting the resonance peaks using finite V_{DS}. For this, we focused on a small interval of V_{BG} (8–35 V) near pinch-off where a number of isolated resonances could be identified. In the (V_{BG},V_{DS}) plane, this leads to diamond-like pattern in differential conductivity dI/dV_{DS} (inset of Figure 3c). The occurrence of transport resonances indicates a rather inhomogeneous charge distribution in MoS_2 films, possibly puddles of charge near conduction threshold, through which charging events at the localized states couple to the metal contacts.

We now turn to the key issue here that concerns the origin of localized states in ultrathin MoS_2 films. This requires an understanding of the origin of disorder in such systems, for which we first examine the values of T_0. However, to compare T_0 for different devices, we define a device-specific reference voltage V_{ON} close to the "pinch-off" voltage in σ *versus* V_{BG} curve, so that the

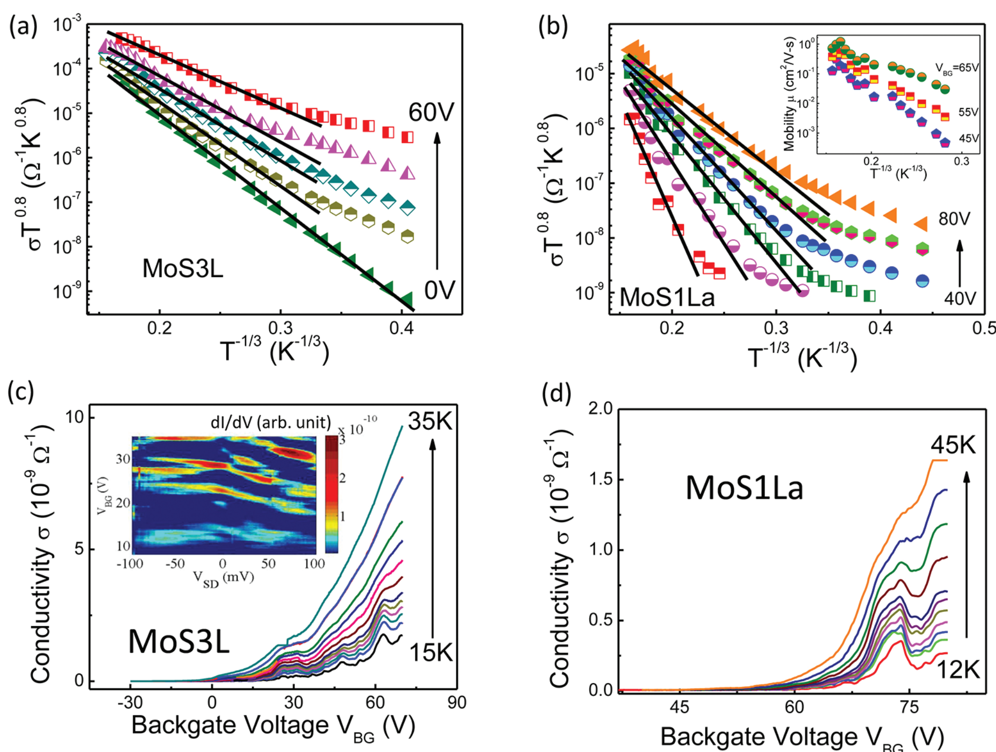

Figure 3. Temperature dependence of conductivity (σ) and variable range hopping (VRH) at different backgate voltages, for (a) MoS3L (V_{DS} = 4 mV) and (b) MoS1La (V_{DS} = 100 mV). The solid black lines are the linear fit to the data indicating VRH behavior in 2D MoS_2 film. Inset in panel b shows variation of mobility (μ) with $T^{-1/3}$ for the single-layer device. (c,d) Reproducible conductance oscillations with backgate voltage (V_{BG}) at low temperature are shown for MoS3L and Mos1La, respectively. Inset of panel c shows the 2D map of the differential conductance dI/dV_{DS} of MoS3L as a function of backgate voltage (V_{BG}) and source−drain bias voltage (V_{DS}) obtained at 12 K.

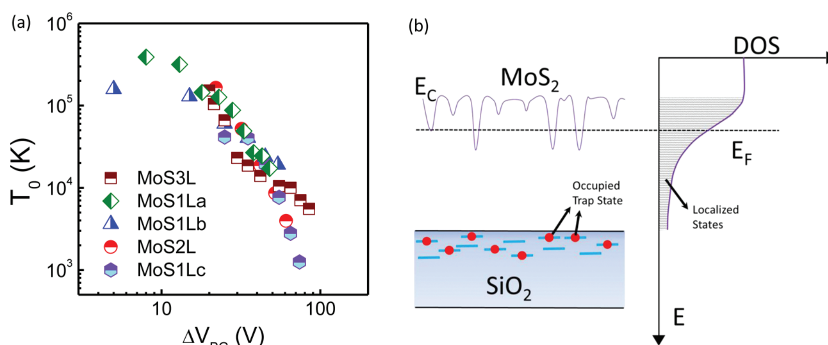

Figure 4. (a) Values of T_0, extracted from VRH slope for five different devices, are plotted as a function of ΔV_{BG} (=$V_{BG} - V_{ON}$). (b) Schematic representation of the fluctuations in the conduction band of MoS_2 thin films, arising due to the proximity of the trapped charges at the SiO_2/MoS_2 interface (left) leading to the band tail and localized states (right).

difference $\Delta V_{BG} = V_{BG} - V_{ON}$ is proportional to E_F or number density n. In Figure 4a, we have plotted the variation of T_0 as a function of ΔV_{BG} for all of the devices. The striking feature here is the close agreement of T_0 in both absolute magnitude and energy over nearly three decades, irrespective of independent preparation of devices, varying layer number, mobility, and device geometry, *etc*. This indicates a very similar disorder landscape in all devices that reflects comparable magnitude and energy dependence of localization length (ξ) and density of states $D(E)$. Disorder arising from defects in bulk of the MoS_2 films is unlikely to explain the insensitivity of T_0 to the number of layers since screening of impurities and density of defect in bulk are expected to strongly influence the density of localized states. Instead, our data indicate a common external origin of disorder, such as the trapped charges in the substrate. This is also supported by recent transport experiments,[4] where higher mobility of thin MoS_2 flakes could be achieved by changing the electrostatic environment alone. Indeed, a charge-trap-induced disorder can readily explain the observed magnitude of T_0. To illustrate this, we take ξ as the typical size of the puddles, which for MoS3L can be roughly estimated to be $\xi \sim 8$ nm from the charging energy (~90 meV) at

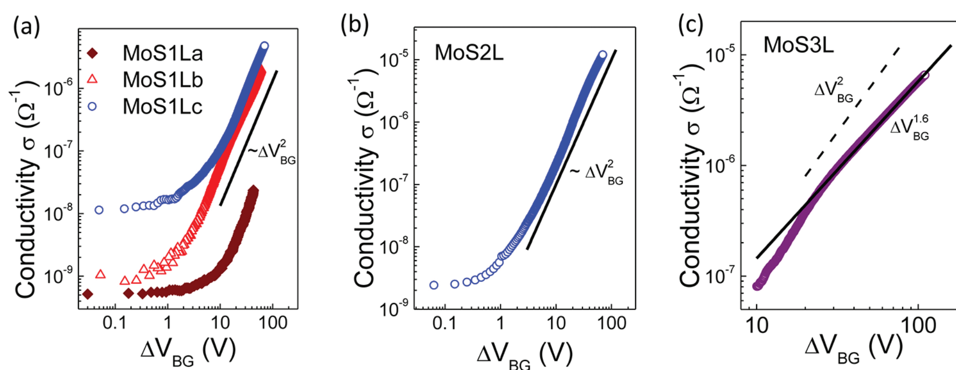

Figure 5. Variation of conductivity σ with ΔV_{BG} for (a) single layer at 240 K (diamond) and 300 K (triangle, circle), (b) bilayer at 300 K, and (c) trilayer at 280 K devices.

$V_{BG} \approx 23$ V (corresponding to $\Delta V_{BG} \approx 48$ V) (see inset of Figure 3c). Taking $D(E) \sim 4 \times 10^{12}$ eV^{-1} cm^{-2} as the typical surface density of charge traps at the SiO_2 interface[11,22] and using $T_0 = 13.8/(k_B\xi^2(E)D(E))$, we find $T_0 \simeq 6.2 \times 10^4$ K, which is in good agreement to the observed magnitude from VRH data (Figure 4a).

This leads us to suggest that the physical origin of the localized states in ultrathin MoS_2 films is connected to the random potential fluctuations from the trapped charges at the MoS_2-SiO_2 interface (see the schematic of Figure 4b). The screening of these trapped charges will be poor due to the large band gap of MoS_2 (unlike graphene) and hence can lead to a considerably long band tail. It is likely that the interfacial traps are randomly occupied during processing of the devices, predominantly *via* transfer of electrons from the exfoliated pristine MoS_2 layers, and subsequently form the frozen disorder landscape since most experiments are conducted at low T.

Finally, to confirm the charge-impurity-induced disorder, we have examined the nature of scattering of carriers by defects at high V_{BG} and T so that the electron wave functions are nearly extended. If the main source of disorder arises from the randomly occupied interfacial traps, one would expect the scattering to be dominated by charge impurity scattering, which for two-dimensional electron systems with parabolic energy bands will lead to[23]

$$\sigma \propto n^2, \text{ bare Coulomb impurity} \quad (2)$$

$$\propto n, \text{ screened Coulomb impurity} \quad (3)$$

In Figure 5a–c, we have shown the dependence of σ on ΔV_{BG} ($\propto n$) near room temperature for the single-layer, bilayer, and trilayer MoS_2 devices, respectively. In all monolayer MoS_2 devices, as well as the bilayer (MoS2L) case, we find $\sigma \propto \Delta V_{BG}^2$, indicating scattering from nearly unscreened charged impurities. In the trilayer device (MoS3L), the variation in $\sigma \sim \Delta V_{BG}^{1.6}$ is somewhat slower, indicating partial screening of the charge impurities. Assuming the electronic density of states to be approximately 1/10 of the free electron density of states at maximal doping ($\sim 5 \times 10^{12}$/cm^2) used in our experiment, the Debye screening length in our devices can be estimated to be ~1.5–2 nm, which is nearly three molecular layers of MoS_2. This readily explains the bare charge impurity scattering in single-layer and bilayer MoS_2, while charge impurities are partially screened for the trilayer device.

It is then natural to draw an analogy of our findings to other heavily researched exfoliated atomic scale transistors, in particular, graphene and topological insulators. The ubiquity of surface trap states probably constitutes a generic source of disorder in such ultrathin field-effect devices. Reducing substrate traps, for example, by using crystalline substrates such as graphene on boron nitride, may improve the quality of these systems considerably. A suspended device, as in case of graphene, could also lead to extremely high mobilities.

CONCLUSION

We have studied low-temperature electrical transport in monolayer, bilayer, and trilayer MoS_2 transistors exfoliated onto Si/SiO_2 substrates. We find that the electrons in all cases are localized well up to room temperature at most gate voltages and display variable range hopping transport as temperature is lowered. We showed that the disorder is likely to arise from Coulomb potential of randomly distributed charges at the MoS_2-SiO_2 interface, and hence highly improved devices should be possible with appropriate substrate engineering.

METHODS

Device Fabrication. MoS_2 flakes were exfoliated from bulk MoS_2 (SPI Supplies) using scotch tape on SiO_2 (300 nm)/n^{++}-Si wafer. To keep the disorder level comparable, the wafers were thoroughly cleaned by standard RCA cleaning followed by acetone and isopropyl alcohol cleaning in ultrasonic bath. The flakes with typical linear dimensions ranging from 2 to 20 μm

were identified by an Olympus BX51 optical microscope. Raman spectra were recorded using a WITEC confocal (100× objective) spectrometer with 600 lines/mm grating, 514.5 nm excitation at a very low laser power level (less than 1 mW) to avoid any heating effect. The AFM measurements were carried out in contact mode with a NT-MDT NTEGRA AFM instrument. Ti(10 nm)/Au(40 nm) or Au(40 nm) contacts were defined using standard electron beam lithography followed by thermal evaporation and lift off in hot acetone. No Ar/H_2 annealing was done in any of our devices.

Acknowledgment. We acknowledge Department of Science and Technology (DST) for a funded project. S.G. and A.N.P. thank CSIR for financial support.

Supporting Information Available: Detailed room temperature and low-temperature drain−source characteristics are presented for trilayer and monolayer devices in Figure S1. The temperature-dependent data for Mott-type variable range hopping for MoS1Lc are shown in Figure S2 along with the calculation of the VRH slope. This material is available free of charge *via* the Internet at http://pubs.acs.org.

REFERENCES AND NOTES

1. Splendiani, A.; Sun, L.; Zhang, Y.; Li, T.; Kim, J.; Chim, C.-Y.; Galli, G.; Wang, F. Emerging Photoluminescence in Monolayer MoS_2. *Nano Lett.* **2010**, *10*, 1271–1275.
2. Mak, K. F.; Lee, C.; Hone, J.; Shan, J.; Heinz, T. F. Atomically Thin MoS_2: A New Direct-Gap Semiconductor. *Phys. Rev. Lett.* **2010**, *105*, 136805.
3. Lee, C.; Yan, H.; Brus, L. E.; Heinz, T. F.; Hone, J.; Ryu, S. Anomalous Lattice Vibrations of Single- and Few-Layer MoS_2. *ACS Nano* **2010**, *4*, 2695–2700.
4. Radisavljevic, B.; Radenovic, A.; Brivio, J.; Giacometti, V.; Kis, A. Single-Layer MoS_2 Transistors. *Nat. Nanotechnol.* **2011**, *6*, 147–150.
5. Pal, A. N.; Ghosh, A. Resistance Noise in Electrically Biased Bilayer Graphene. *Phys. Rev. Lett.* **2011**, *102*, 126805.
6. Pal, A. N.; Ghatak, S.; Kochat, V.; Sneha, E. S.; Sampathkumar, A.; Raghavan, S.; Ghosh, A. Microscopic Mechanism of 1/f Noise in Graphene: Role of Energy Band Dispersion. *ACS Nano* **2011**, *5*, 2075–2081.
7. Efros, A. L.; Pikus, F. G.; Samsonidze, G. G. Maximum Low-Temperature Mobility of Two-Dimensional Electrons in Heterojunctions with a Thick Spacer Layer. *Phys. Rev. B* **1990**, *41*, 8295–8301.
8. Adam, S.; Hwang, E. H.; Rossi, E.; Das Sarma, S. Theory of Charged Impurity Scattering in Two-Dimensional Graphene. *Solid State Commun.* **2009**, *149*, 1072–1079.
9. Martin, J.; Akerman, N.; Ulbricht, G.; Lohmann, T.; Smet, J. H.; Klitzing, K. v.; Yacoby, A. Observaion of Electron-Hole Puddles in Graphene Using a Scanning Single-Electron Transistor. *Nat. Phys.* **2008**, *4*, 144–148.
10. Baenninger, M.; Ghosh, A.; Pepper, M.; Beere, H. E.; Farrer, I.; Atkinson, P.; Ritchie, D. A. Local Transport in a Disorder-Stabilized Correlated Insulating Phase. *Phys. Rev. B* **2005**, *72*, 241311.
11. Ayari, A.; Cobas, E.; Ogundadegbe, O.; Fuhrer, M. S. Realization and Electrical Characterization of Ultrathin Crystals of Layered Transition-Metal Dichalcogenides. *J. Appl. Phys.* **2007**, *101*, 014507.
12. Novoselov, K. S.; Jiang, D.; Schedin, F.; Booth, T. J.; Khotkevich, V. V.; Morozov, S. V.; Geim, A. K. Two-Dimensional Atomic Crystals. *Proc. Natl. Acad. Sci. U.S.A.* **2005**, *102*, 10451–10453.
13. Novoselov, K. S.; Geim, A. K.; Morozov, S. V.; Jiang, D.; Zhang, Y.; Dubonos, S. V.; Grigorieva, I. V.; Firsov, A. A. Electric Field Effect in Atomically Thin Carbon Films. *Science* **2004**, *306*, 666–669.
14. Paasch, G.; Lindner, T.; Scheinert, S. Variable Range Hopping as Possible Origin of a Universal Relation between Conductivity and Mobility in Disordered Organic Semiconductors. *Synth. Met.* **2002**, *132*, 97–104.
15. Mott, N. F.; Davis, E. A. *Electronic Processes in Non-crystalline Materials*; Clarendon Press: Oxford, 1971.
16. Van Keuls, F. W.; Hu, X. L.; Jiang, H. W.; Dahm, A. J. Screening of the Coulomb Interaction in Two-Dimensional Variable-Range Hopping. *Phys. Rev. B* **1997**, *56*, 1161–1169.
17. The Efros-Shklovskii-type variable range hopping with ln $\sigma \propto T^{-1/2}$ was also considered. However, the data were found to have much better agreement with ln $\sigma \propto T^{-1/3}$ in almost all cases.
18. Pepper, M.; Pollitt, S.; Adkins, C. J. The Spatial Extent of Localized State Wavefunctions in Silicon Inversion Layers. *J. Phys. C: Solid State Phys.* **1974**, *7*, L273–L277.
19. Ghosh, A.; Pepper, M.; Ritchie, D. A.; Linfield, E. H.; Harrell, R. H.; Beere, H. E.; Jones, G. A. C. Electron Assisted Variable Range Hopping in Strongly Correlated 2D Electron Systems. *Phys. Status Solidi B* **2002**, *230*, 211–216.
20. Fowler, A. B.; Timp, G. L.; Wainer, J. J.; Webb, R. A. Observation of Resonant Tunneling in Silicon Inversion Layers. *Phys. Rev. Lett.* **1986**, *57*, 138–141.
21. Ghosh, A.; Pepper, M.; Beere, E. B.; Ritchie, D. A. Density-Dependent Instabilities in Correlated Two Dimensional Electron Systems. *J. Phys. C: Condens. Matter* **2004**, *16*, 3623–3631.
22. Jayaraman, R.; Sodini, C. G. A 1/f Noise Technique To Extract the Oxide Trap Density near the Conduction Band Edge of Silicon. *IEEE Trans. Electron Dev.* **1989**, *36*, 1773.
23. Adam, S.; Das Sarma, S. Boltzmann Transport and Residual Conductivity in Bilayer Graphene. *Phys. Rev. B* **2008**, *77*, 115436.